

Positioning the Angle of Attack Sensor on an Unmanned Aerial Vehicle Wing

Amir Hossein Birjandi^{1,*}, Valentin Guerry¹, Eric Bibeau¹, Hamidreza Bolandhemmat², and Kaiwen Xu²

¹University of Manitoba, Winnipeg, Manitoba, Canada

²Micropilot Corporation, Winnipeg, Manitoba, Canada

Abstract: Two vane type angle of attack sensors, small and large, are tested on the suction surface of a wing of an unmanned aerial vehicle to evaluate the wing interference with angle of attack reading. Tests are performed in the University of Manitoba's wind tunnel with the maximum Reynolds number of 4.5×10^5 to find the optimal location to place sensors on the wing. Each angle of attack sensor is tested at four positions on the wing to investigate the impact of flow deflection caused by the presence of the wing on the sensor readings. Results show that readings are highly sensitive to the normal clearance between the wing and the angle of attack sensor. Accuracy of sensor readings increases by increasing normal clearance. Spanwise placements indicate that the minimum wing interference with angle of attack sensor readings occurs when the sensor is placed beyond the wing tip. To investigate the effect of ailerons on angle of attack sensor readings, sensors are also tested with half, full and with no aileron deflection positions. The effect of aileron deflection is noticeable in large angle of attack sensor readings, while it has a negligible effect on the small sensor readings.

Keywords: UAV, angle of attack sensor, flow Interaction, wind tunnel testing.

1. INTRODUCTION

Unmanned aerial vehicles (UAVs) used for civilian and military applications are continuously expanding and their missions are increasing in task and complexity. To answer the need for complex missions, UAVs have to be equipped with accurate sensors coupled to advanced processing software. Large UAVs are normally equipped with sensors to indicate the wind velocity, Angle Of Attack (AOA) and the sideslip angle. Such parameters are required to estimate the aerodynamic loads and to derive the flight dynamic coefficients by solving the six degree of freedom equations of motion to simulate the flight of an UAV [1, 2]. Although small UAVs usually do not require such sensors, an accurate AOA sensor is becoming essential to develop autopilots for small UAVs with more complex missions. Without accurate measurements, the autopilot software must rely on calibrated AOA estimating methods using kinematic relationships to navigate [3-7]. Moreover, to reduce flight test risks and costs, it is recommended to obtain such calibration in a wind tunnel and implement the AOA estimation method in a hardware-in-the-loop simulation to predict UAV performance and dynamic behavior [8, 9]. Unlike large UAVs, it is challenging to find a fully developed flow region on small UAVs where flow gradients are zero.

Vane type AOA sensors are common for commercial planes. This type of sensor is low cost robust and simple to operate. Such sensor is normally located on a zero pressure gradient region on the fuselage where there is fully developed flow and no curvature [10]. For single propeller tractor UAVs, the fuselage is not an option to install the AOA sensor since it is in the downwash of the propeller. For this type of UAV, it is recommended to install the sensor on the pressure side of the wing, lower side of the wing. For UAVs without a landing gear this location is not practical since the sensor will be damaged during the landing process. For this type of UAV, the upper side of the wing remains the only option to install the sensor. In this study different locations on the upper side of an UAV wing are investigated to find a place with minimum wing interaction to install AOA sensors.

2. EXPERIMENTAL SETUP

Two vane-type AOA sensors are tested on a UAV wing in the wind tunnel at the University of Manitoba. The large AOA sensor is 23.2cm long located on a 14.2cm stem; as shown in Figure 1, the small AOA sensor is 8.3cm long located on a 2.7cm stem. The wing used in tests has a S712 cross-section profile with 8.12% maximum thickness, as shown in Figure 2. The wing chord length is 30cm and has a 120cm span.

3. WIND TUNNEL VELOCITY CALIBRATION

The wind tunnel shown in Figure 3 is a closed loop wind tunnel with an open test section. The cross

*Address correspondence to this author at the University of Manitoba, Winnipeg, Manitoba, Canada; Tel: 204-9512399; Fax: 204 275 7507; E-mail: amir.birjandi@gmail.com

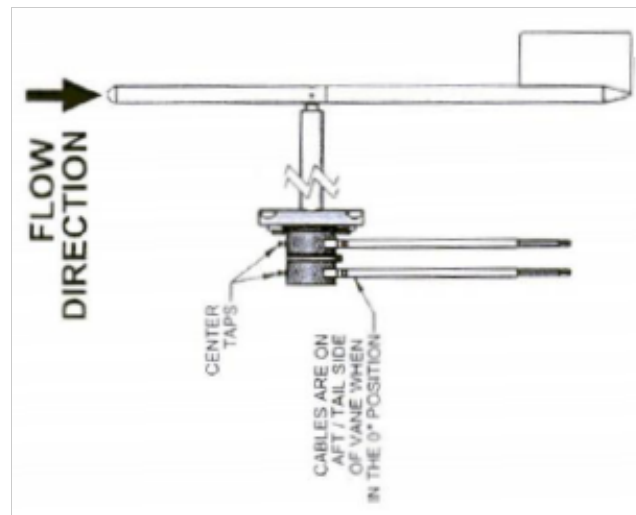


Figure 1: Vane type AOA sensor used for UAV applications.

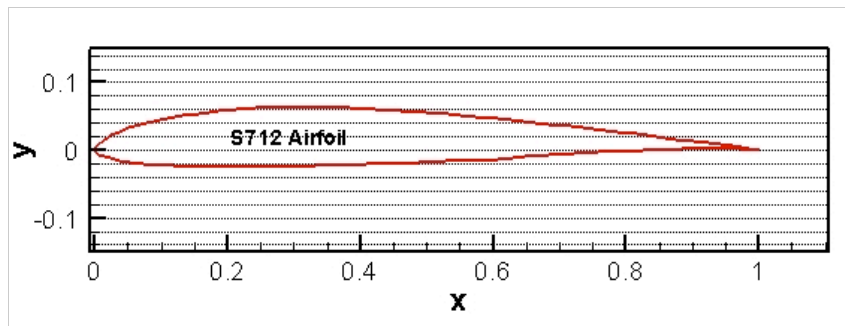


Figure 2: Wing S712 cross section profile used in AOA sensor placement study.

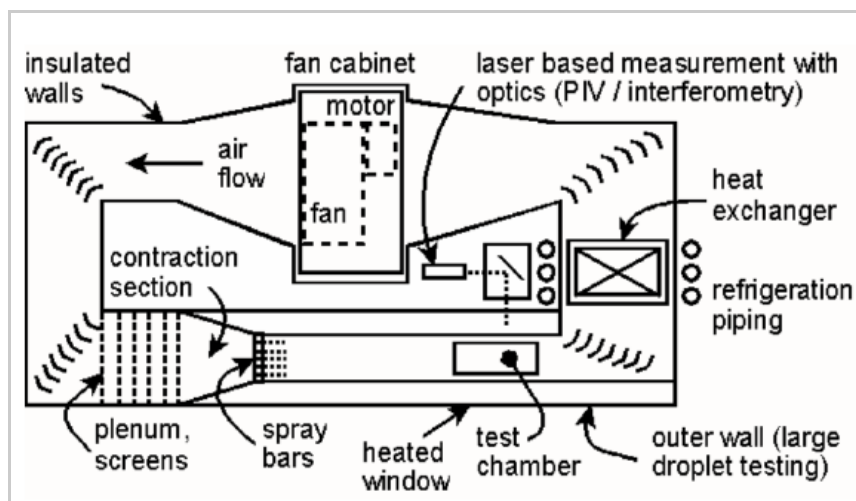


Figure 3: Schematic plan view of the wind tunnel.

section of the test-section is 1m wide by 1m high. It is capable of circulating air in the test section at the maximum speed of 30m/s. Before conducting tests on the AOA sensors, air speed in the cross section of the test section is calibrated using a Pitot tube to identify

air flow uniformity at the test section. Results are shown in Table 1. A variable frequency drive controls the air speed in the test section. Measurements show that the average air speed at the center of the test section changes linearly with the frequency of the drive.

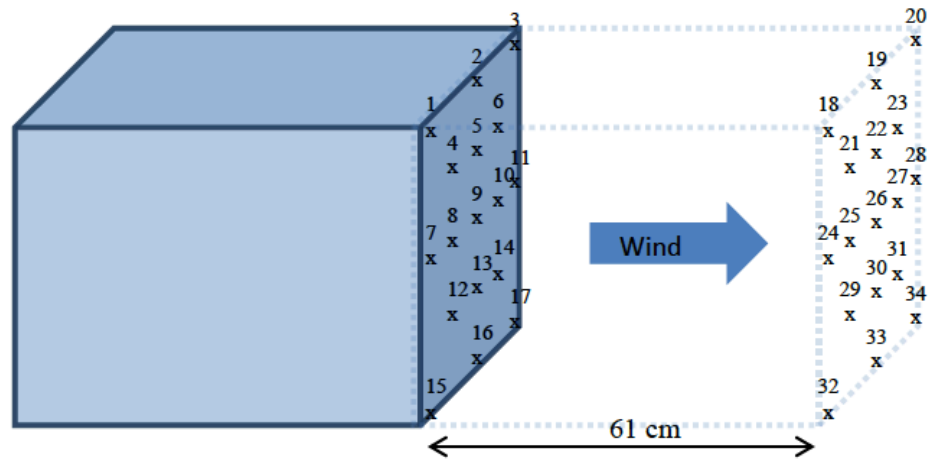


Figure 4: Measurement point locations for wind tunnel flow uniformity verification.

Table 1: Air Speed and Temperatures at the Center of the Wind Tunnel

Motor frequency (Hz)	Measured air speed (m/s)	Temperature (°C)
20.0	10.0	27.2
40.0	21.0	27.2
50.0	26.0	26.6

To find an area with the most uniform air speed distribution, the air speed is measured on two parallel planes, one at the exit section of the wind tunnel test section and second one 61cm downstream of the test section exit in the open area of the tunnel. Air speed is measured at 17 points on each plane, as shown in Figure 4.

Velocity measurement results are presented in Table 2. Air velocity is uniformly distributed in the wind tunnel test section except near walls due to the presence of the boundary layer. The velocity drop between the first and second plane is less than 4% and is attributed to the expansion occurring when the flow reaches the open section at the end of the test section.

4. AOA SENSOR ACCURACY IN FREE FLOW

AOA sensors are tested in the wind tunnel in free flow with no wing. This test is performed in the center area of plane 2 where the air speed is uniform, as shown in Table 3. In this test, the large sensor is tested at AOAs between -40° and +40° with 10° increments (with respect to the air flow). The small AOA sensor is tested at AOAs between -30° and +30° with 10° increments. The narrower test range for the small AOA sensor is due to the operational limitations of this

sensor. The test setup is shown in Figure 5. Results are presented in Figure 6. Measured AOAs with two sensors have less than 2° deviation from the actual AOA for all investigated velocities.

At air velocities less than 7m/s, the response time of the large sensor to change in AOA is high. It requires more than 10s to adjust itself to the new AOA. The accuracy of the large sensor therefore decreases at lower velocities—the weight of the large sensor is relatively high and requires more torque to rotate and adjust itself to new conditions. The amount of torque on the vane is proportional to the velocity square of the air flow; therefore, at low air velocities the amount of torque on the vane is low thereby the response time of the sensor is high. In addition to inertia, frictional losses reduce the accuracy of the large sensor at lower velocities. For velocities from 7 to 14m/s, the large sensor accuracy improves but the response time remains high, more than 5s to adjust itself with new angle. For air velocities above 14m/s, the large sensor is accurate and the response time is within the acceptable range.

The small AOA sensor operation range is between -30° and 30°. Results in Figure 6 show that the small sensor is accurate within 1° deviation from the actual AOA. In comparison to the results for the large sensor, the small AOA sensor has less inertia and frictional resistance. Therefore, even at low air velocities it is accurate and has a fast response time to changes in AOA. However, when the air velocity increases beyond 9.5m/s, the sensor becomes unstable and vibrates considerably: the sensor fluctuates by approximately +/- 5°. The results in Figure 6 are the averaged results; therefore do not reflect of the fluctuating nature of the data. The unsteadiness of the small AOA sensor is the

Table 2: Velocity Distribution in the Test Section

Point # See Figure 1	Frequency Drive Setting (Hz)										
	5	10	15	20	25	30	35	40	45	50	55
Plane 1 Velocity (m/s)											
1	0.7	2.1	3.4	4.9	6.3	7.5	8.9	10.4	11.9	13.3	15.0
2	1.0	2.6	4.5	6.6	8.5	10.5	12.5	14.4	16.4	17.8	20.6
3	0.7	2.0	3.4	4.8	6.3	7.8	9.2	10.6	12.0	13.5	15.2
4	1.7	4.3	7.1	9.8	12.7	15.6	18.4	21.3	23.8	26.4	29.0
5	1.7	4.4	7.0	9.8	12.6	15.5	18.5	21.5	24.0	26.5	29.2
6	1.7	4.3	7.0	9.7	12.6	15.4	18.4	21.2	23.8	26.5	29.0
7	0.9	2.4	4.0	5.7	7.5	9.0	10.7	12.3	14.1	15.9	17.5
8	1.8	4.3	6.8	9.5	12.5	15.3	18.2	20.8	23.6	26.2	29.0
9	1.9	4.3	7.0	9.7	12.6	15.4	18.4	21.0	23.6	26.3	29.1
10	1.6	4.1	6.6	9.3	12.2	15	17.7	20.5	23.0	25.7	28.5
11	1.0	2.5	4.2	5.8	7.6	9.3	10.9	12.5	14.3	16.2	17.8
12	1.6	4.0	6.7	9.5	12.1	14.9	17.7	20.4	23.0	25.7	28.4
13	1.7	4.1	6.9	9.3	12.1	14.7	17.6	20.2	22.7	25.6	28.0
14	1.6	4.1	6.7	9.5	12.2	14.9	17.7	20.2	22.9	25.5	28.2
15	0.8	2.3	3.6	5.4	6.8	8.3	9.8	11.5	13.1	14.5	15.9
16	1.1	3.0	5.0	7.1	9.0	11	13.1	15	16.7	18.8	20.8
17	0.8	2.1	3.5	5.1	6.7	8.2	9.7	11.3	12.7	14.3	15.7
Plane 2 Velocity (m/s)											
18	1.2	2.9	4.9	6.8	8.5	10.4	11.2	13.0	14.7	15.2	16.8
19	1.1	3.4	5.5	7.5	10.4	12.4	14.3	15.8	17.6	19.0	20.3
20	1.3	3.0	5.0	6.9	8.4	10.5	11.0	13.0	14.5	15.3	17.0
21	1.6	3.9	6.6	9.3	11.9	14.4	16.9	19.3	22.2	24.5	26.6
22	1.6	4.0	6.4	9.0	11.5	14.0	16.6	19.1	21.5	24.2	26.5
23	1.7	4.2	6.8	9.6	12.3	15.3	18.2	20.8	22.7	24.8	26.6
24	1.1	3.3	5.8	8.5	10.7	12.8	14.6	16.2	18.4	20.0	21.4
25	1.6	3.8	6.2	9.0	11.5	14.0	16.4	19.3	21.7	24.3	26.5
26	1.7	4.0	6.5	9.3	12	14.5	17.1	19.7	22.5	25.0	27.0
27	1.7	4.2	6.8	9.7	12.3	14.9	17.2	19.6	22.4	25.0	27.0
28	1.0	2.6	4.5	6.6	8.5	10.5	12.5	14.4	16.4	17.8	20.4
29	1.5	3.8	6.2	9.0	11.4	14.0	16.3	18.6	21.4	24.0	26.4
30	1.6	4.0	6.5	9.0	11.6	14.3	16.6	19.0	21.9	24.5	27.2
31	1.5	3.7	6.0	8.9	11.3	13.9	16.3	18.3	21.2	23.8	26.2
32	1.1	2.6	4.5	6.0	7.8	9.4	11.4	13.3	15.2	16.8	18.4
33	1.0	2.7	4.5	6.1	7.8	9.5	11.5	13.4	15.3	17.0	18.6
34	1.0	2.5	4.3	5.8	7.6	9.2	11.2	13.1	15.0	16.6	18.2



Figure 5: Test setup for AOA sensors in the wind tunnel with no wing.

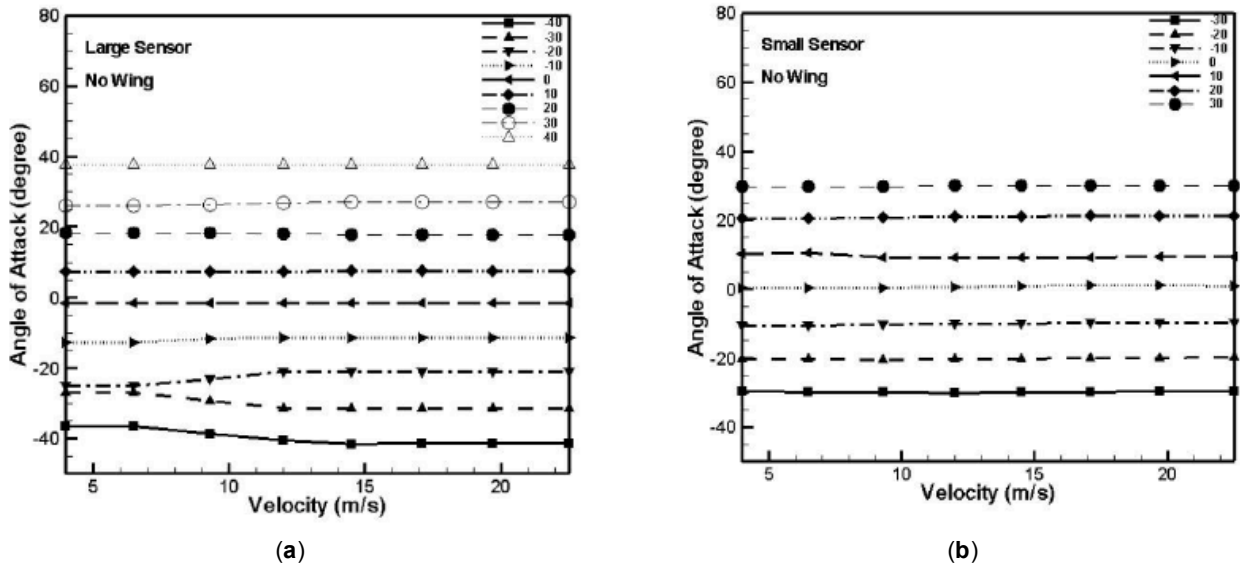


Figure 6: Test performed in free flow comparing results obtained with the, (a) large AOA sensor, and (b) small AOA sensor.

result of the flow instability passing over a hinged vane with low inertia and low friction. Eddies with length scales comparable with the vane dimension can create asymmetrical pressure on the vane and cause fluctuation in the system. Despite the unsteady behaviour of the small AOA sensor, the average value is more accurate compared to the output of the large AOA sensor.

5. WING SENSOR INTERACTION

The interaction between the wing and the AOA sensors are presented in this section. Sensors are placed on the suction, upper surface, of the UAV wing. Figure 7 shows the test setup and Table 3 summarizes the four positions, P1 to P4, of the sensors with respect to the wing. In position P1 the sensor is placed 8cm from the leading edge of the wing, 34cm inside the

wing from the wing tip, and 4.5cm above the wing. Measurements are conducted at various air velocities and different angles of attack to identify the wing interference with AOA sensor readings. To position sensors accurately on the upper side of the wing, a mount system is developed to rotate the sensor and the wing simultaneously. Therefore, sensors and the wing experience the same AOA during the test. The wing-sensor assembly is capable of rotating $\pm 40^\circ$ about its rotating axis. The rotating axis is located at 1/4 of the chord length measured from the leading edge of the wing. In this study, the AOA of the system is changed by 10° increments, spanning -40° to $+40^\circ$. At every AOA position the large AOA sensor is tested at 6 air velocities from 9.7m/s to 22.4m/s, while the small AOA sensor is tested at 9 air velocities over the same velocity range.



Figure 7: Setup for large AOA sensor located on the upper surface of the wing: (a) wing and sensor, (b) wind tunnel test section and wing fixed on a stand.

Table 3: Sensor Positions P1 to P4 with Respect to the Wing for Measurement of Impact of Sensor Location

Figure label	Distances (cm)	P1	P2	P3	P4
A	From leading edge	8	8	8	8
B	From wing tip	34	48	48	-4
C	Wing proximity	4.5	4.5	14.5	1.5

6. RESULTS FOR THE LARGE SENSOR INTERACTION WITH THE WING

When the large AOA sensor is tested at location P1 at various angles of attack and air speeds, all sensor readings are negative, even for positive wing angles of attack, as shown in Figure 8a. At position P1 the large AOA sensor is under the influence of the flow pattern on the wing and unable to track the AOA of the wing as the air flow curves over the suction side of the wing. Therefore, the flow pattern on the suction side of the wing pushes the tail of the sensor downwards, which is located near the trailing edge of the wing. This effect is prominent at positive angles of attack. Due to the close proximity of the sensor to the wing, the tail of the large

AOA sensor hits the wing at near -25° . The large AOA sensor demonstrates an unsteady behavior in interaction with the wing. Therefore, even at small angles of attack, like -20° , the tail of the sensor hits the wing in some occasions and affects sensor reading accuracy. The area below the horizontal dashed line in Figure 8 indicates the AOA region where the tail of the large sensor contacts the wing at position P1 and P2. Results obtained for position P1 show that for any AOA beyond the $\pm 10^\circ$ range, the sensor hits the wing. This occurs at higher air velocities for the negative angles of attacks; however for the positive angles of attacks it occurs for the whole velocity range. The trend is the same for position P2. Therefore the large AOA sensor is unable to track the real AOA (Figure 8b).

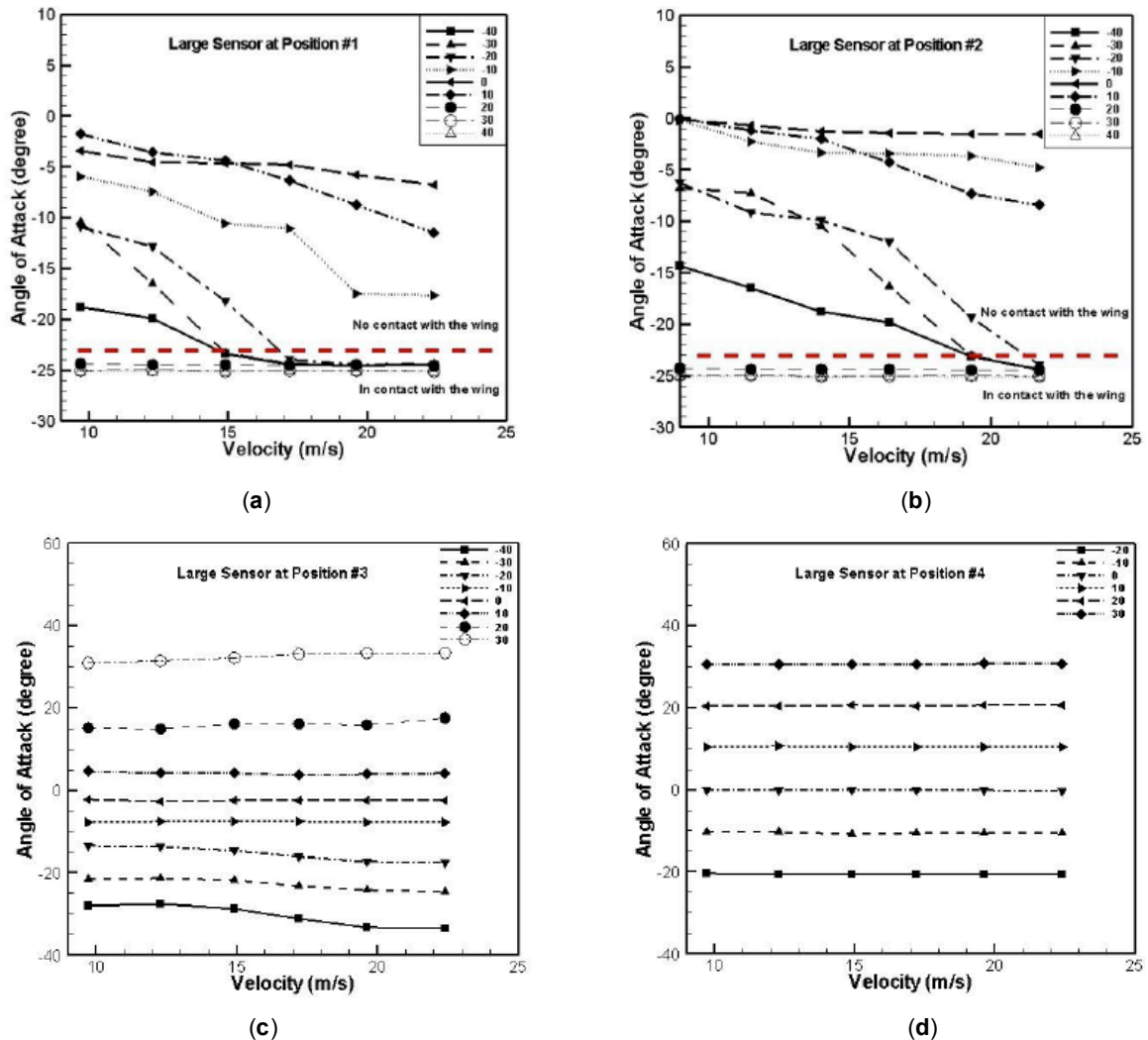


Figure 8: Large sensor results for 9 angles of attack from -40° to 40° investigated over a velocity range of 9 to 25 m/s and sensors located at positions, (a) P1, (b) P2, (c) P3 and, (d) P4. The red line shows when the sensor contacts the wing.

By moving the AOA sensor to position P3, the readings are improved, Figure 8c. Readings are now more consistent although the values are still inaccurate with deviations between 2.5° to 12° . At position P3 there is no contact between the sensor and the wing. Finally, the large AOA sensor is placed at position P4 which is 4cm outside of the wing. In this position, the wing proximity is 1.5cm which limits the operation angle of the large attack sensor between -20° to $+30^{\circ}$. At this position the large AOA sensor has the most accurate readings compared to previous positions tested, Figure 8d. The largest deviation between the sensor readings and the actual angles of attack at position P4 is about 0.7° .

7. RESULTS FOR SMALL SENSOR INTERACTION WITH THE WING

The small sensor is tested at velocities in the range of 1.7m/s and 22.4m/s. Results for the small sensor are

shown in Figures 9. In position P1 and P2, results in Figure 9a show reduction in sensor accuracy as the air velocity increases. At P1 and P2, the AOA readings approaches zero as the air velocity increases, Figure 9a and 9b. This effect is more prominent at position P1. The behavior of the small AOA sensor is stable up to the air velocity of 10 m/s, but beyond that the air velocity, the sensor starts fluctuating. At high air velocities the amplitude of fluctuations reaches 4° .

In position P3, the readings of the AOA sensor shown in Figure 9c are improved and the unsteady behavior of the sensor occurs at air velocities higher than 15m/s and the fluctuation amplitudes are damped and become lower than 2° . For negative angles of attack at air speed exceeding 5m/s sensor readings experience a positive jump. In this position, the error is less than 1° for positive angles of attack but the error reaches 12° for negative angles of attack and high

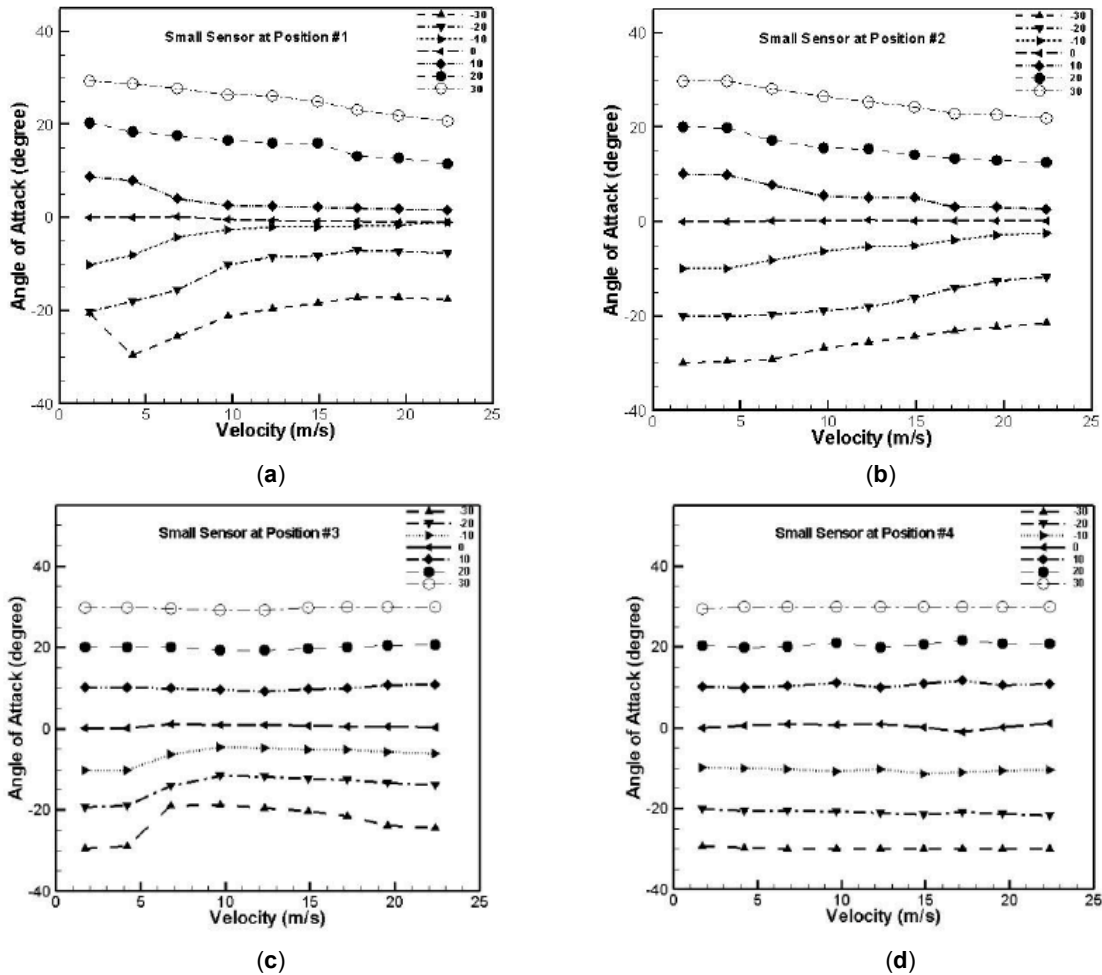


Figure 9: Small sensor AOA results for 7 angles of attack between -30° to 30° investigated over a velocity range spanning from 1.7 to 22.4m/s when located at positions (a) P1, (b) P2, (c) P3 and, (d) P4.



Figure 10: Aileron positions, (a) no deflection, (b) half deflection, and (c) full deflection.

velocities. Like the large sensor, the small sensor has the highest accuracy at position P4, located outside of the wing. In this position the error is less than 1° , Figure 9d.

8. AILERON INTERACTION

In the final series of tests AOA sensors are tested against the effect of the aileron deflection. In this investigation the AOA of the wing is set to zero and

sensors are placed in position P2 (see Table 1). Three aileron deflections are applied to the wing: no deflection, half deflection, and full deflection, as shown in Figure 10. Figure 11 shows the effect of the aileron deflection on the AOA readings for both sensors. Figure 11a shows the large sensor is highly sensitive to the aileron deflection. Half and full aileron deflections cause the large AOA sensor to read negative AOAs. The same test is conducted using the small AOA

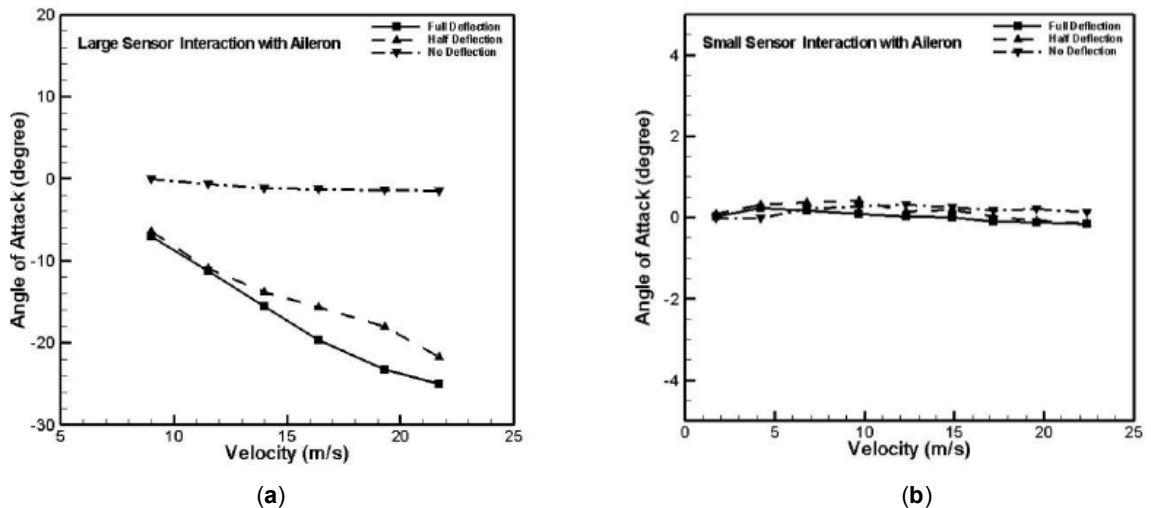


Figure 11: Aileron deflection effect on the, (a) large AOA sensor and (b) small AOA sensor.

sensor and results are presented in Figure 11b. Results indicate negligible effect of aileron deflection on the small AOA sensor readings.

CONCLUSIONS

In this study two vane-type AOA sensors with different sizes are tested in the wind tunnel to investigate the interaction between the wing and the sensors. The goal of this study is to find the optimum location to place the AOA sensor on the suction side of the wing for small UAVs. Sensors are tested in three positions along the span and two proximity distances from the wing upper surface. Results showed that the large AOA sensor has slow response time and is not accurate at low air velocities due to high inertia and friction. The small AOA sensor is more accurate compared to the large AOA but readings are unsteady at higher velocities. Results for different positions on the wing show that by increasing the distance between the wing and sensor accuracy of readings are improved. The optimum location for AOA sensor is outside of the wing at position P4. Finally, aileron deflection affects the large AOA reading results while it has a negligible effect on the small AOA sensor.

REFERENCES

- [1] Stevens BL and Lewis FL. Aircraft Control and Simulation. John Wiley and Sons, Hoboken, NJ, 2nd ed., 2003.

- [2] Etkin B and Reid LD. Dynamics of Flight: Stability and Control. John Wiley and Sons. New York, NY, 3rd ed., 1996.
- [3] Beard RW and McLain TW. Small Unmanned Aircraft: Theory and Practice. Princeton University Press 2012. <http://dx.doi.org/10.1515/9781400840601>
- [4] Ramprasad C and Arya H. Multi-stage fusion algorithm for estimation of aerodynamic angles in mini aerial vehicle. in Proc. 49th AIAA Aerospace Science Meeting, Orlando, FL, 2011. <http://dx.doi.org/10.2514/6.2011-1287>
- [5] Cho A, Kim V, Lee S and Kee C. Wind estimation and airspeed calibration using a UAV with a single-antenna GPS receiver and pitot tube. IEEE Trans. Aerospace and Electronic Systems 2011; 47: 109-117. <http://dx.doi.org/10.1109/TAES.2011.5705663>
- [6] Cho A, Kang YS, Park BJ and Yoo CS. Airflow angle and wind estimation using GPS/INS navigation data and airspeed. in Proc. 13th Int. Conf. Control, Automation and Systems (ICCAS), Gwangju, Korea, 2013. <http://dx.doi.org/10.1109/iccas.2013.6704159>
- [7] Johansen TA, Cristafaro A, Sørensen KL, Hansen JM and Fossen TI. On estimation of wind velocity, angle-of-attack and sideslip angle of small uavs using standard sensors. In International Conference on Unmanned Aircraft Systems 2015. <http://dx.doi.org/10.1109/icuas.2015.7152330>
- [8] Johnson EN and Fontaine S. Use of Flight Simulation to Complement Flight Testing of Low-cost UAVs. AIAA Modeling and Simulation Technologies Conference and Exhibit. Montreal, Canada 2001; AIAA 2001-4059.
- [9] Sorton EF and Hammaker S. Simulated Flight Testing of an Autonomous Unmanned Aerial Vehicle Using FlightGear. Infotech@Aerospace, Arlington, VA 2005; AIAA 2005-7083.
- [10] Gracey W. Summary of methods of measuring AOA on aircraft 1958.